



Biological Effects of Double-Layered Hydroxyapatite and Zirconium Oxide Depositions on Titanium Surfaces

Min-Kyung Ji ^{1,*}, Yaerim Chun ^{2,*}, Geonwoo Jeong³, Hyun-Seung Kim⁴, Won-Jae Kim⁵, Je-Hwang Ryu⁶, Hoonsung Cho ³, Hyun-Pil Lim^{1,2}

¹Dental 4D Research Center, Chonnam National University, Gwangju, Republic of Korea; ²Department of Prosthodontics, School of Dentistry, Chonnam National University, Gwangju, Republic of Korea; ³Department of Materials Science and Engineering, Chonnam National University, Gwangju, Republic of Korea; ⁴KJ Meditech Co., Ltd, Gwangju, Republic of Korea; ⁵Department of Oral Physiology, School of Dentistry, Stem Cell Secretome Research Center, Chonnam National University, Gwangju, Republic of Korea; ⁶Department of Pharmacology and Dental Therapeutics, School of Dentistry, Chonnam National University, Gwangju, Republic of Korea

*These authors contributed equally to this work

Correspondence: Hyun-Pil Lim, Department of Prosthodontics, School of Dentistry, Chonnam National University, Gwangju, 61186, Republic of Korea, Tel +82-10-2645-7528, Fax +82-62-530-5577, Email mcnihil@jnu.ac.kr; Hoonsung Cho, Department of Materials Science and Engineering, Chonnam National University, Gwangju, 61186, Republic of Korea, Tel/Fax +82-62-530-1717, Email cho.hoonsung@jnu.ac.kr

Purpose: This study aimed to confirm the synergy effect of these two materials by evaluating osteoblast and antibacterial activity by applying a double-layered hydroxyapatite(HA) zirconium oxide(ZrO₂) coating to titanium.

Methods: The specimens used in this study were divided into four groups: a control group (polished titanium; group T) and three experimental groups: Group TH (RF magnetron sputtered HA deposited titanium), Group Z (ZrO₂ ALD deposited titanium), and Group ZH (RF magnetron sputtered HA and ZrO₂ ALD deposited titanium). The adhesion of *Streptococcus mutans* (*S.mutans*) to the surface was assessed using a crystal violet assay. The adhesion, proliferation, and differentiation of MC3T3-E1 cells, a mouse osteoblastic cell line, were assessed through a WST-8 assay and ALP assay.

Results: Group Z showed a decrease in the adhesion of *S. mutans* ($p < 0.05$) and an improvement in osteoblastic viability ($p < 0.0083$). Group TH and ZH showed a decrease in adhesion of *S. mutans* ($p < 0.05$) and an increase in osteoblastic cell proliferation and cell differentiation ($p < 0.0083$). Group ZH exhibited the highest antibacterial and osteoblastic differentiation.

Conclusion: In conclusion double-layered HA and ZrO₂ deposited on titanium were shown to be more effective in inhibiting the adhesion of *S. mutans*, which induced biofilm formation, and increasing osteoblastic differentiation involved in osseointegration by the synergistic effect of the two materials.

Keywords: zirconium oxide, hydroxyapatite, atomic layer deposition, radio frequency magnetron sputter, osteoblast activity, antibacterial effect

Introduction

As the population ages, the number of people suffering from bone defects or bone diseases is increasing, resulting in the rising demand for various biomedical implants. Titanium (Ti) is the most widely used implant material due to its mechanical strength and good biocompatibility. However, the lack of bioactivity and antibacterial properties of titanium can lead to loose fixations with bones and postoperative infections.¹ Moreover, the oxidized TiO₂ layer formed on the Ti surface is stable enough to make the surface bio-inert.² Surface modifications are widely used to enhance the bioactivity and improve the antibacterial properties of the Ti surface of dental implants.³

Surface modifications to create bioactive and antibacterial dental implant surfaces have been attempted, and several biological properties have been shown to be improved. Zirconium oxide is used for dental materials due to its tooth-like appearance and unique mechanical properties, such as the ability to decrease peri-implant inflammation.⁴ Scarano et al

reported that zirconium oxide-coated titanium surfaces had a reduction in bacterial attachment and biofilm accumulation, thereby reducing the occurrence of inflammatory reactions.⁵ Atomic layer deposition (ALD) is a surface modifying method based on two consecutive and cyclic self-saturating reactions. It is used to fabricate nanometer-scaled layers on different substrates such as bioinert and rough materials. It provides precise thickness control and has excellent uniformity.^{6,7} Due to the surface morphology of dental implants, which have regular threads on their surface, it is critical to form a uniform layer that remains stable on complex structures. Jo et al fabricated titanium surfaces with zirconium oxide using ALD. Zirconium oxide ALD on titanium surfaces has been shown to inhibit bacterial adhesion and improve osteoblastic viability.⁸

Hydroxyapatite (HA, $\text{Ca}_{10}(\text{PO}_4)_6(\text{OH})_2$) is one of the natural components of bone and teeth and has structural and chemical similarities to natural bone. HA is a bioactive material with high biocompatibility, making it a commonly used coating material for surface modifications of dental implants.¹ Radio frequency (RF) magnetron sputtering is a deposition technique that can be used to form dense, uniform, and solid HA coatings at a thickness of less than 1 μm , with equally distributed structure and composition. These sputtered HA coatings have been shown to have in vivo and in vitro bioactive characteristics on Ti surfaces.⁹ Previous studies have reported that the three main advantages of preparing a coating by magnetron sputtering are a controlled thickness and uniform coating, a tightly bonded film, and various types of ingredients can be added to the coating and the morphology of the coatings can be easily controlled.¹⁰

Previous studies have reported that zirconium oxide-based surfaces inhibit bacterial adhesion compared with untreated titanium surfaces. Also, zirconium oxide is known to be an inert biomaterial.⁴ However, there have been no studies that have fabricated and evaluated the combination of zirconium oxide ALD titanium treated and RF magnetron sputtered HA surfaces. Thus, this study aimed to confirm the synergy effect of these two materials by evaluating the osteoblast and antibacterial activity by applying a double-layer hydroxyapatite zirconium oxide coating to titanium. In this study, HA coating was formed on titanium surfaces and zirconium oxide-coated titanium surfaces by the RF magnetron sputtering technique. There were two null hypotheses. The first null hypothesis was that double-layered hydroxyapatite zirconium oxide coating on titanium would not inhibit biofilm formation. The second null hypothesis was that double-layered hydroxyapatite zirconium oxide coating on titanium would have no effect on osteoblast activation.

Materials and Methods

Experimental Materials

Specimen Preparation

A total of 48 pure titanium (ASTM Grade IV, Kobe Steel, Kobe, Japan) discs 15 mm in diameter and 3 mm thick were prepared for each group. The titanium discs were polished with 600-, 800-, and 1000-grit SiC abrasive papers under running water. The titanium discs were ultrasonically cleaned in acetone, ethanol, and distilled water for 15 minutes each and then dried.

Zirconium Oxide Atomic Layer Deposition

An ALD system (Compact ALD 150, ULTECH Co., Ltd., Daegu, Korea) was used to deposit nanoscale zirconium oxide onto the titanium surface. TEMAZr (tetrakis[ethylmethylamido]zirconium(IV)); Zr40-001, UP Chem., Gyeonggi-do, Korea) was used as a precursor, H_2O was used as a reactant, and high-purity Ar (99.999%) was used as a carrier gas. The processing temperature was set to 200°C to maintain a constant growth rate and avoid impurities forming due to thermal decomposition. A total of 150 cycles were performed on the titanium surface (Table 1).

Table 1 Processing of Atomic Layer Deposition Zirconium Oxide

Processing Temperature (°C)	Ar ₂ Flow rate (SCCM)	ALD Sequence				Growth Cycle
		TEMAZr Pulse(s)	Ar ₂ Purge(s)	H ₂ O Pulse(s)	Ar ₂ Purge(s)	
200	350	0.05	50	0.5	50	150

Hydroxyapatite Deposition

The magnetron sputtering mechanism involves HA target and the interaction of ions with the substrate. The basic sputtering is processed as following: (1) the neutral gas is ionized by an external power supply, producing a glow discharge (ie a partially ionized gas) or plasma; (2) a source (the target) is bombarded with gas ions in high vacuum; (3) atoms from the target are ejected and then diffuse through the chamber; (4) a thin layer is formed by atomic deposition on the substrate (Figure 1).

The Ti surfaces were deposited with HA by an RF magnetron sputtering unit (ATS-MC-STD-300, A-Tech system, Korea) with the use of HA target and argon gas. The argon gas flow rate was 30 SCCM. The base pressure and working pressure was 7.0×10^{-1} Pa. The sputtering distance between substrate and HA target was 8 cm. The process was performed with RF power of 100 W, for 60 minutes after pre-sputtering of 5 minutes. After the formation of the HA coating, the specimens were not heat-treated.

Double-Layered Hydroxyapatite and Zirconium Oxide Depositions

HA was additionally deposited onto the ZrO_2 deposited discs to create a double-layer hydroxyapatite zirconium oxide coating surface.

Classification of the Experimental Groups

The specimens used in this study were divided into a control group (polished titanium; Group T) and three experimental groups: Group TH (RF magnetron sputtered HA deposited titanium), Group Z (ZrO_2 ALD deposited titanium), and Group ZH (RF magnetron sputtered HA and ZrO_2 ALD deposited titanium) (Table 2).

Assessment of Surface Characteristics

The surface morphology and thickness of HA and zirconium oxide deposited on the specimens were observed using a field emission scanning electron microscope (FE-SEM; S-4700, Hitachi, Horiba, Japan). The elemental changes of the surfaces after HA and zirconium oxide deposition were observed using FE-SEM equipped with energy-dispersive X-ray spectroscopy (EDS; EX-220, Horiba, Ltd., Kyoto, Japan) ($n = 1$) and X-ray photoemission spectroscopy (XPS; MultiLab 2000, Thermo Electron Co., England) ($n = 1$). Surface roughness tests were performed using a 2D contact stylus profilometer (DIAVITE DH-8, ASMETO LTD, Bülach, Switzerland). Average roughness (R_a) was measured at three points on each specimen. The average surface roughness of each group was calculated as the average R_a of three specimens per group ($n = 3$). The comparison of surface hydrophilicity of each group was performed through a contact angle measurement ($n = 6$). Distilled water, as a polar liquid, and diiodomethane (99%), as a nonpolar liquid, were used

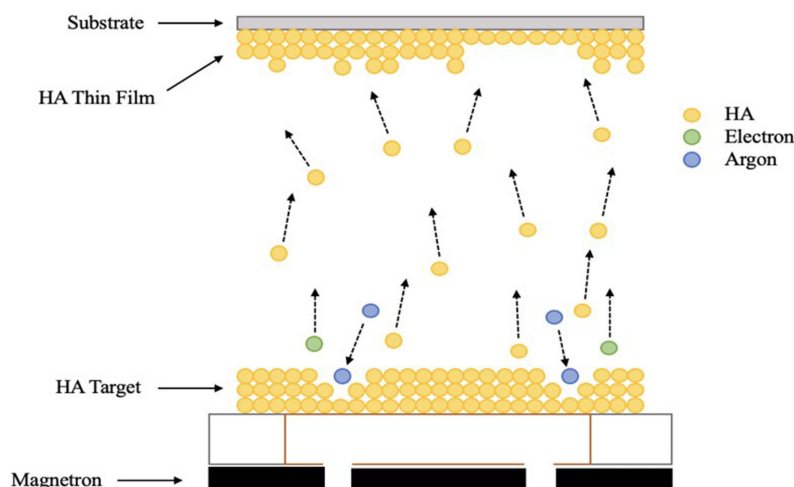


Figure 1 Schematic diagram of the sputtering mechanism.

Table 2 Experimental Groups in This Study

Group	Zirconium Oxide Deposition	HA Deposition
T	No treatment	No treatment
TH	No treatment	RF magnetron sputtered HA coating
Z	Zirconium oxide ALD	No treatment
ZH	Zirconium oxide ALD	RF magnetron sputtered HA coating

as solvents. Each solvent was dispensed on the surface of the specimen in the amount of 15 μ L, and the contact angle was measured with a video contact angle measuring device (Phoenix 300, SEO, Yongin, Korea). The average was calculated by measuring the contact angle of three specimens per each experimental group in each solvent. Surface free energy (SFE) was also calculated with the obtained contact angle values. The calculation was performed using the Owens-Wendt method.¹¹ Table 3 lists the previously reported values for the SFE of water and diiodomethane.¹²

Assessment of Inhibition of Bacterial Formation

Bacterial Culture

The inhibition of biofilm formation was assessed using the gram-positive bacterium *Streptococcus mutans* (KCOM 1504), which causes early biofilm formation. *S. mutans* strains were purchased from the Korean Collection for Oral Microbiology (KCOM, Gwangju, Korea). Brain Heart Infusion broth (BHI, Becton, Dickinson and Company, Sparks, MD, USA) was used as the culture medium. A single colony of *S. mutans* formed on the solid medium was transferred into the liquid medium and cultured in an incubator (LIB-150M, DAIHAN Labtech Co., Korea) at 37°C.

Bacterial Inoculation

Seven specimens per group were located in a 24-well plate, and *S. mutans* suspension was prepared at a concentration of 1.5×10^7 CFU/mL. *S. mutans* were inoculated on the specimens and cultured for 24 hours in a 37°C incubator.

Bacterial Formation Assessment

Biofilm formation was assessed using a crystal violet staining assay. *S. mutans* were cultured on the surface of the specimens. After 24 hours, the unattached bacteria were washed out twice with a PBS solution, 0.3% Crystal violet solution (Sigma-Aldrich, St. Louis, MO, USA) was dispensed onto the specimens, and the specimens were dyed for 10 minutes. The crystal violet solution was then removed, and the specimens were washed three times with PBS and dried for 15 minutes. A destaining solution (80% ethyl alcohol and 20% acetone) was dispensed onto the dried specimens and stirred for one hour. Then destaining solution was placed into a 96-well plate. The absorbance was measured at 595 nm using a microplate spectrophotometer (Epoch2, BioTek, Winooski, VT, USA).

Table 3 Surface Energies (γ) and Their Dispersive (γ_d) and Polar (γ_p) Components

Liquid	Surface Energy (mN/m)		
	γ	γ_d	γ_p
Water	72.8	21.8	51
Diiodomethane	50.8	50.8	0

Assessment of Osteoblast Viability

Cell Culture

The mouse preosteoblastic cell line MC3T3-E1 Subclone 4 (ATCC CRL2593, Rockville, MD, USA) was purchased from the American Type Culture Collection (ATCC; Manassas, VA, USA). The cells were cultured in α -Minimum Essential Medium (α -MEM; Gibco-BRL, Grand Island, NY, USA) supplemented with 10% fetal bovine serum (FBS) and 100 U/mL of penicillin. The cells were cultured at 37°C in a 5% CO₂ incubator (SafeGrow Pro incubator, EuroClone, Pero, Italy). The culture media was replaced every three days, and the MC3T3-E1 cells were subcultured until the number of cells needed for the experiment was obtained.

Cell Adhesion and Proliferation

In total, ten specimens per group were added to a 24-well plate. The osteoblastic cell suspension was prepared at a density of 4×10^4 cells/mL for each well with α -MEM, and the plates were cultured at 37°C in a 5% CO₂ incubator. The cells were cultured for 24 hours for the cell attachment analysis and five days for the cell proliferation analysis. For the cell attachment and proliferation analyses, a WST-8 assay (EZ-Cytox, Itsbio Inc., Seoul, Korea) was used. The WST-8 reagent was dispensed into each well, and the plates were incubated at 37°C in a 5% CO₂ incubator. When the medium color changed to orange, 100 μ L of the culture medium containing the reagent from each well was transferred into a 96-well plate. The absorbance was measured at 450 nm using a microplate spectrophotometer (Epoch2, BioTek, Winooski, VT, USA).

Cell Differentiation

The MC3T3-E1 cells used in the differentiation assay were conditioned the same as the attachment and proliferation assay. The cells were cultured for 14 days. For the analysis of cell differentiation, an Alkaline phosphatase (ALP) assay was used. The ALP assay buffer reagent (200 μ L; Biovision Inc., Milpitas, CA, USA) was distributed to each specimen, and the plate was incubated at 37 °C in a 5% CO₂ incubator for one hour. The pNPP solution (50 μ L; Biovision Inc., Milpitas, CA, USA) was added to each well and cultured in an incubator for one hour. The stop solution (Biovision Inc., Milpitas, CA, USA) was added to each well. The absorbance was measured at 405 nm using a microplate spectrophotometer.

Statistical Analysis

All statistical analyses in this study were performed using SPSS version 27.0 (SPSS Inc., Chicago, IL, USA). In case of biofilm formation data, normality was satisfied according to a Shapiro–Wilk test, a one-way ANOVA was used to test the parameters. A Duncan test was used as the post-hoc test. The significance level was 95% and was considered statistically significant when the *p*-value was less than 0.05. In case of osteoblast activation data, normality was not satisfied, statistical differences between the test groups were evaluated using the Kruskal–Wallis test as a nonparametric method. A Mann–Whitney test was followed as the post-hoc test to perform a comparison between groups. Type I errors were corrected using Bonferroni’s method. The significance of all data collected was tested at a significance level of *p* < 0.0083.

Results

Surface Characteristics

In the FE-SEM observations, nanoparticles of zirconium oxide were observed to form a monogenous layer in group Z. It was also observed that in Group TH and ZH, particles of HA were deposited uniformly and that in Group ZH, the zirconium oxide particles formed on the surface were covered by the deposited HA (Figure 2). As a result of depositing zirconium oxide and HA on Si-wafers and observing the thickness, the thickness of zirconium oxide and HA was 26nm and 77 nm, respectively, and the thickness of the double layered zirconium oxide and HA was about 103nm (Figure 3). In the EDS analysis, it was confirmed that the zirconium oxide and HA layers were formed through zirconium (Zr), calcium (Ca), and phosphate (P) peaks on the surface (Figure 4).

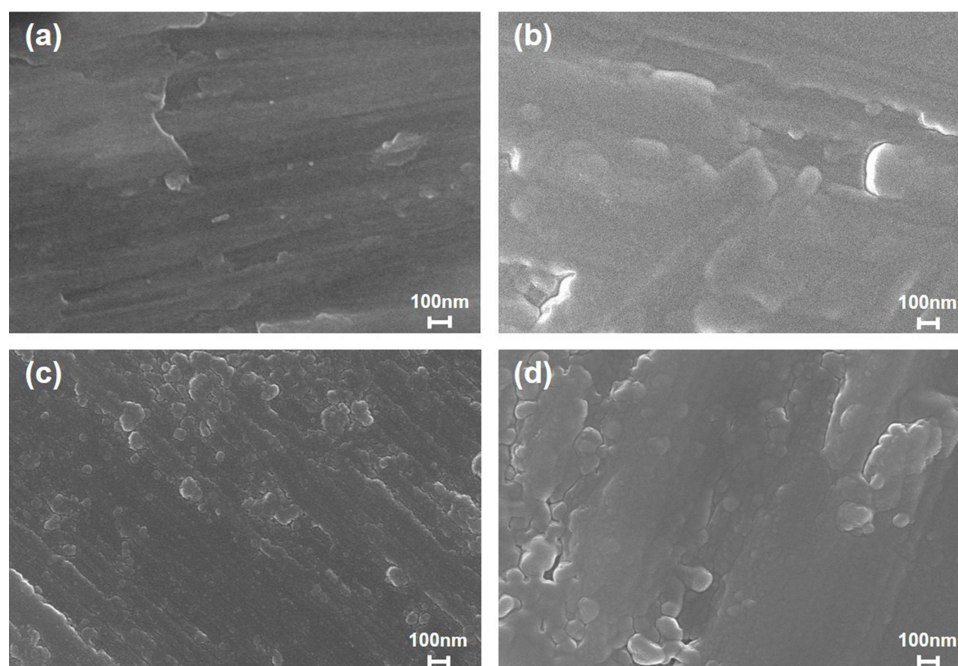


Figure 2 Field emission-scanning electron microscopy images on group (a) T, (b) TH, (c) Z, and (d) ZH (magnification = 50,000).

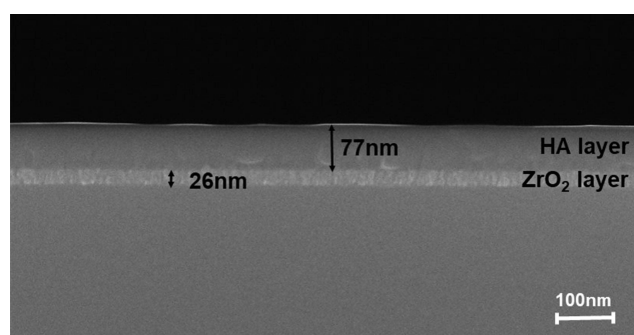


Figure 3 Field emission-scanning electron microscopy images of deposition thickness on Si-wafers (magnification = 100,000).

The results of the chemical composition analysis of the zirconium oxide and HA deposits are shown in [Figure 5](#). The general XPS survey spectrum of the zirconium oxide and HA deposits exhibited the Zr3d, Ca2p and P2p bands ([Figure 5a](#) and [b](#)). After zirconium oxide deposition, the spin-orbit doublet Zr3d peak (182.1, 184.9 eV) detected in the Ti samples reflects zirconium oxide ([Figure 5c](#)). After HA deposition, the Ca2p (346.7, 350.2 eV) and P2p (132.8) peaks detected in the Ti samples reflect HA ([Figure 5d](#) and [e](#)). The peak at 346.7 eV indicates the possibility of one or more calcium-containing compounds, such as $\text{Ca}_3(\text{PO}_4)_2$, CaO, CaHPO_4 , or HA. The binding energy peak at 350.2 eV corresponds to the energy peak of Ca in CaCO_3 . In the case of P2p3/2, the peak observed at 133.6 eV corresponds to $(\text{PO}_4)_3^-$ ([Figure 5e](#)). In Group ZH, the Zr3d peak was not detected, and the P2s (190.1 eV) peak detected in Group ZH reflects $(\text{PO}_4)_3^-$. In the case of Ca2p and P2p, the same binding energy peaks in group TH were detected.

The change in contact angle according to zirconium oxide and HA deposition is shown in [Figures 6](#) and [7](#). The water contact angle was measured to be $76.5 \pm 1.6^\circ$ for Group T, $28.0 \pm 2.6^\circ$ for Group TH, $95.6 \pm 0.9^\circ$ for Group Z, and $25.5 \pm 0.9^\circ$ for Group ZH. The zirconium oxide deposited surface had an increased water contact angle, and the HA deposited surface had a reduced water contact angle. The diiodomethane contact angle was measured to be $46.3 \pm 2.8^\circ$ for Group T, $44.1 \pm 1.7^\circ$ for Group TH, $44.6 \pm 2.6^\circ$ for Group Z, and $34.6 \pm 1.8^\circ$ for Group ZH. The change in SFE according to

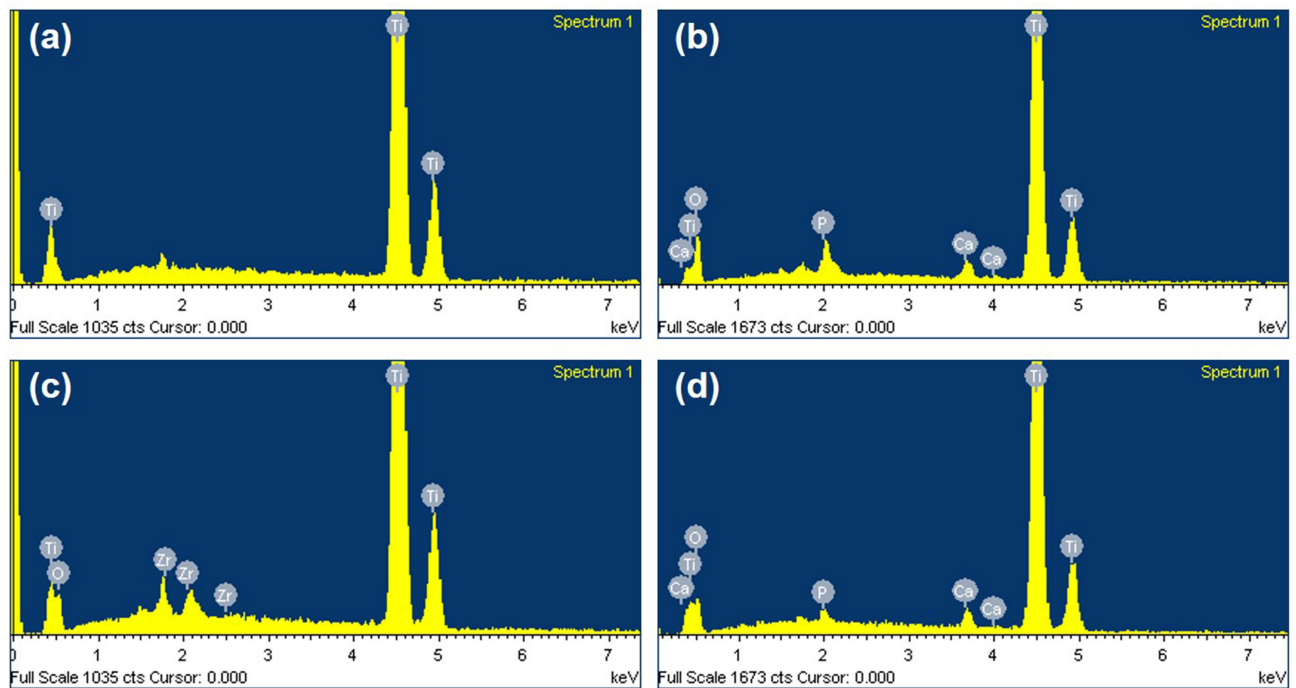


Figure 4 Energy Dispersive spectroscopy (EDS) spectra of the zirconium oxide and HA layers on group (a) T, (b) TH, (c) Z, and (d) ZH.

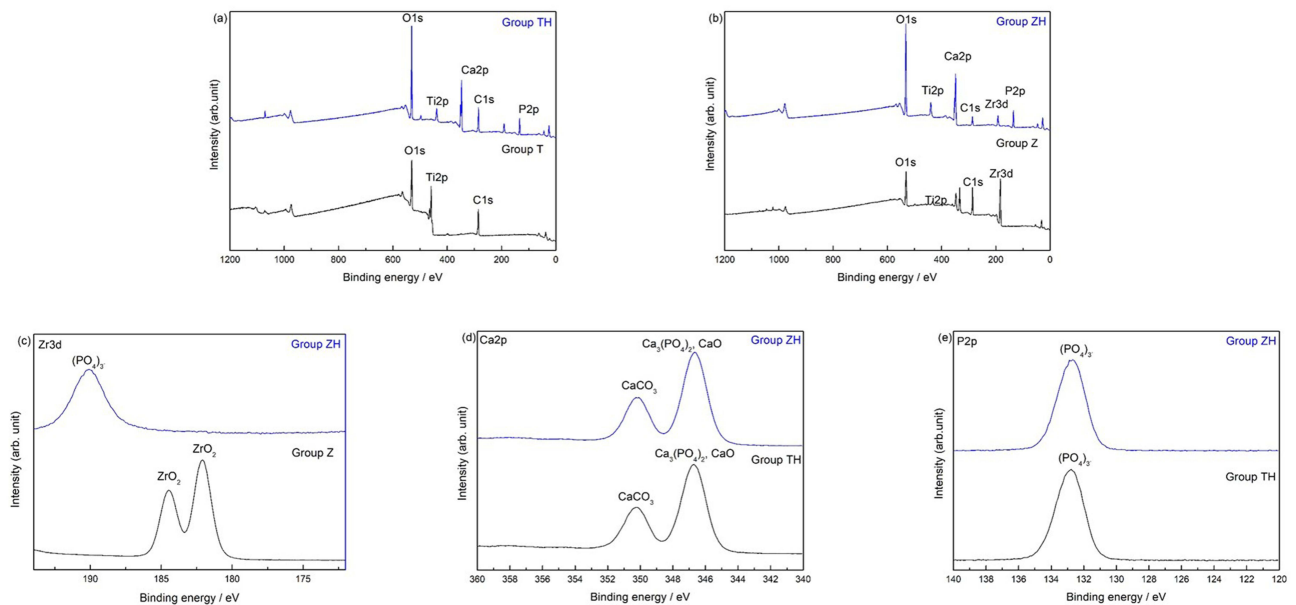


Figure 5 Chemical composition analysis of zirconium oxide and HA depositions: (a and b) survey XPS spectrum, narrow scans of (c) Zr3d, (d) Ca2p, and (e) P2p.

zirconium oxide and HA deposition is shown in Figure 8. The total SFE was calculated to be 41.5 mN/m for Group T, 68.3 mN/m for Group TH, 37.9 mN/m for Group Z, and 70.3 mN/m for Group ZH. The HA deposited surface had a sharp increase in the polar component of the SFE and total SFE.

The Ra was measured to be 288 nm for Group T, 292 nm for Group TH, 282 nm for Group Z, and 300 nm for Group ZH (Figure 9). The Ra of all of the groups was observed between 282 and 300 nm.

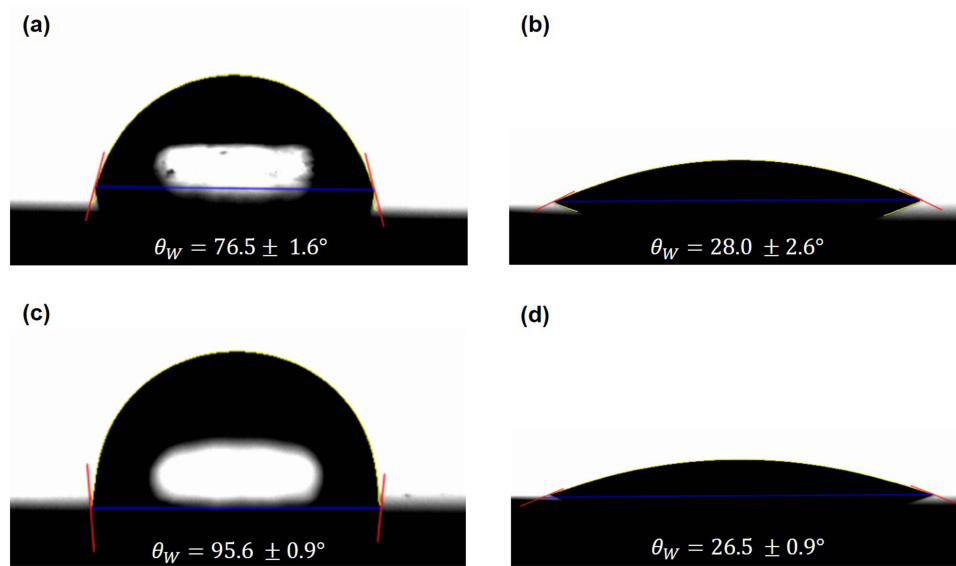


Figure 6 Water contact angle images of group (a) T, (b) TH, (c) Z, and (d) ZH.

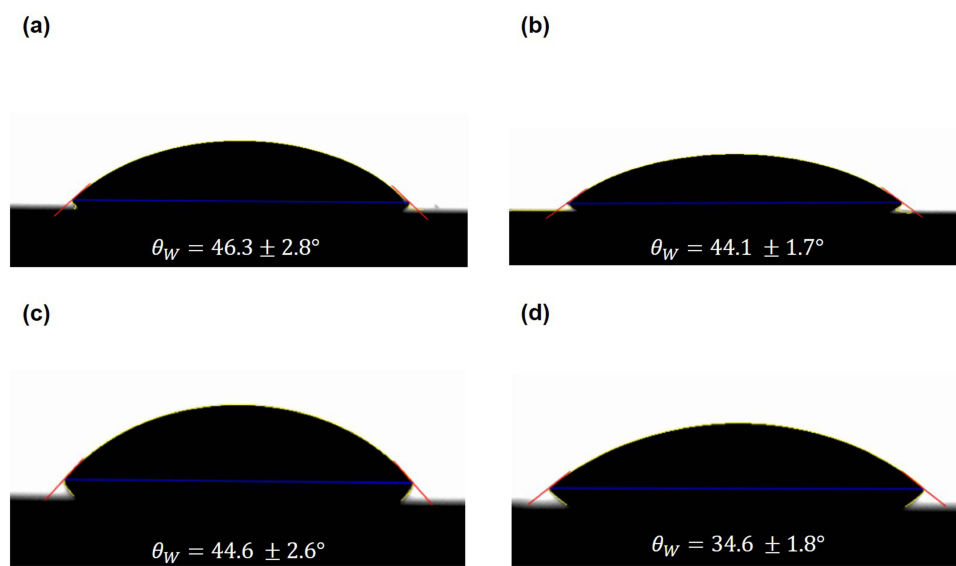


Figure 7 Diiodomethane contact angle images of group (a) T, (b) TH, (c) Z, and (d) ZH.

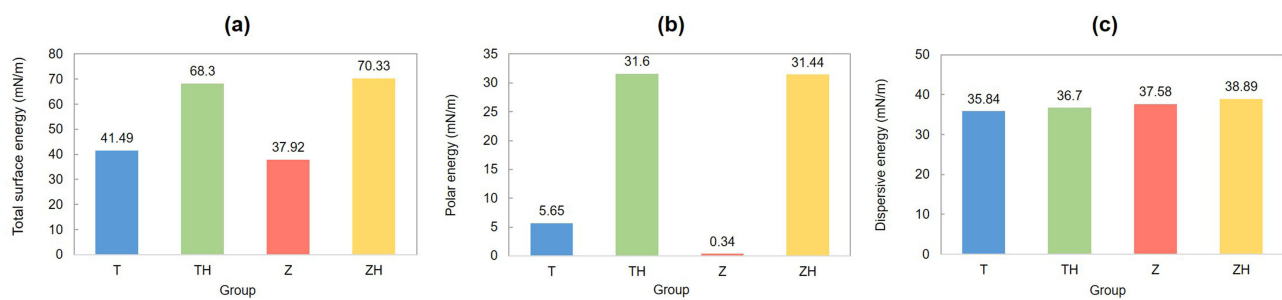


Figure 8 Surface free energy: (a) Total SFE, (b) Polar energy, and (c) Dispersive energy.

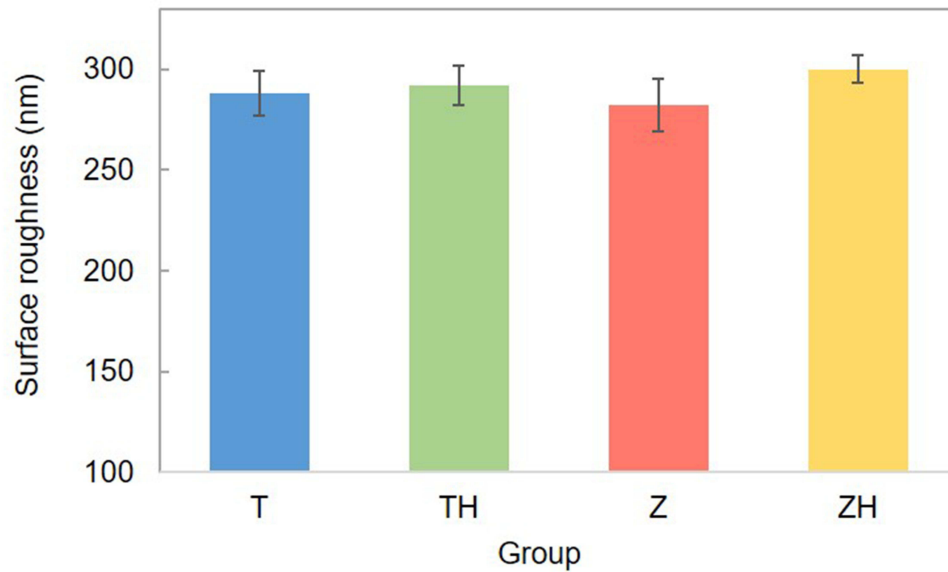


Figure 9 Average roughness (Ra) of each group.

Inhibition of Biofilm Formation

By assessing the biofilm formation of *S. mutans* on the specimens, it was found that adhesion was significantly decreased in the experimental groups (Groups TH, Z, and ZH) compared with the control group (Group T). In addition, the biofilm formation of *S. mutans* in group ZH was significantly lower than in group Z ($p < 0.05$; Figure 10).

Osteoblast Activation

Effects on Cell Adhesion, Proliferation, and Differentiation

The adhesion of MC3T3-E1 cells was significantly increased in Groups Z and ZH compared with Groups T and TH ($p < 0.0083$). There was no significant difference between Groups T and TH and Groups Z and ZH ($p > 0.0083$;

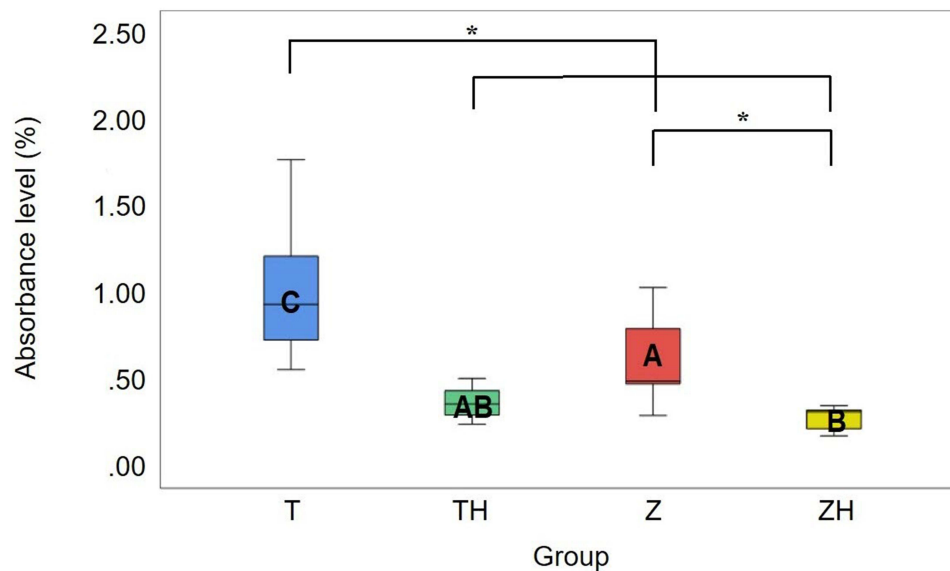


Figure 10 Percentage of absorbance level of *S. mutans* cultured on each group. Different uppercase letters in the graph indicate significant differences (*Significant at $p < 0.05$).

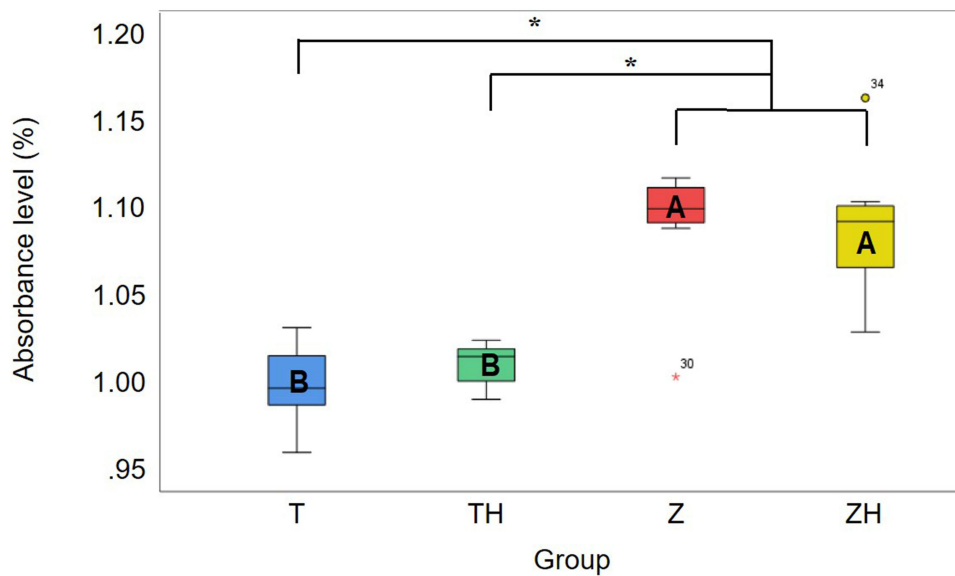


Figure 11 Evaluation of the cell viability of MC3T3-E1 cells in each group. Outliers are denoted by circles. Different uppercase letters in the graph indicate significant differences (*Significant at $p < 0.083$).

Figure 11). The proliferation of MC3T3-E1 cells was significantly increased in the experimental groups (Groups TH, Z, and ZH) compared with the control group (Group T). In addition, the proliferation of the MC3T3-E1 cells in Group ZH was significantly increased compared with the cells in Group Z ($p < 0.0083$; Figure 12). The differentiation of MC3T3-E1 cells was significantly increased in the experimental groups (Groups TH, Z, and ZH) compared with the control group (Group T) ($p < 0.0083$). There was no significant difference between Groups TH, Z, and ZH ($p > 0.0083$; Figure 13).

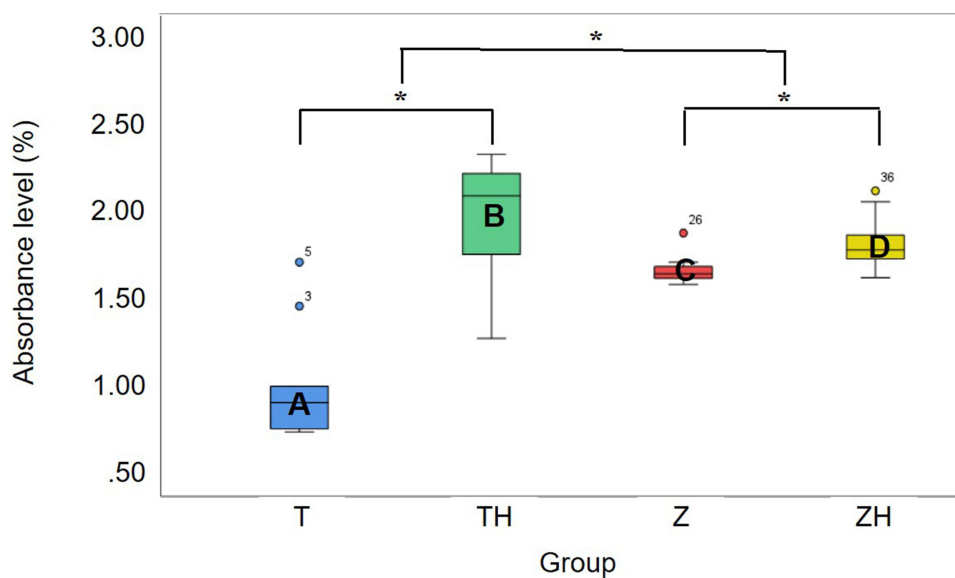


Figure 12 Evaluation of the cell proliferation of MC3T3-E1 cells of each group. Outliers are denoted by circles. Different uppercase letters in the graph indicate significant differences (*Significant at $p < 0.083$).

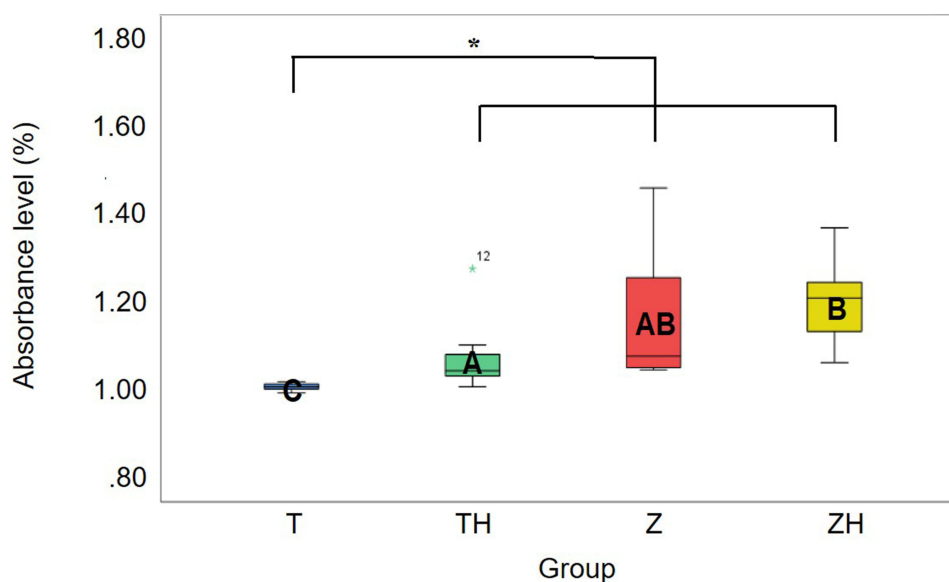


Figure 13 Evaluation of the cell differentiation of MC3T3-E1 cells of each group. Outliers are denoted by circles. Different uppercase letters in the graph indicate significant differences (*Significant at $p < 0.0083$).

Discussion

HA is among the most attractive biomaterials due to its chemical similarity to natural bone and excellent biological properties. The main advantage of HA as a coating material is its bioactive properties, which promote stronger biological fixation to bone tissues.¹³ The crystal structure of HA has been shown to allow small-scale replacement of Ca^{2+} ions with the various foreign ions, which promotes osteoblast adhesion.¹

The surface roughness and the SFE are known to play significant roles in the initial adhesion of bacteria.¹⁴ Higher surface roughness increases the surface area and tends to enhance bacterial adhesion as surface irregularities act as a shelter for the bacteria.^{14,15} The average surface roughness increased with the HA coating; however, bacterial adhesion was decreased. This result can be explained by the increased surface roughness from the HA deposition leads to an abrasive surface texturing, which contributes to the mechanical damage on the bacterial cell membrane.¹⁶

Additionally, *S. mutans*, which was used in this study, is a gram-positive coccus and has a thicker cell wall with more peptidoglycan compared with gram-negative bacteria. Peptidoglycans have been shown to cause more Ca^{2+} ions to be trapped at the surface.¹⁶ The cell wall of *S. mutans* also consists of covalent bonded polypeptides. Studies have shown that these proteins could be a factor that restricts proliferation.¹⁷ Therefore, it is assumed that the destruction of the cell wall and the interactions between the cell wall, surface chemistry, and surface structure formed by HA resulted in the inhibition of bacterial attachment on the HA-deposited surfaces.

In the contact angle observations, compared with Groups T and Z, the water contact angle was decreased, and the surface energy was significantly increased in Groups TH and ZH. The HA-coated surfaces became hydrophilic due to the negative surface charge formed by the abundance of surface hydroxyl groups in HA.¹⁸ This negative charge creates a repulsive force between the surface and the bacteria.¹⁹

Lower surface energy is known to cause less bacterial adhesion; however, the opposite tendency was observed in this study. This result can be explained by the general conception that hydrophobic microorganisms prefer hydrophobic substrates. Hydrophobic interactions have been reported to play an important role in microbial adherence.²⁰ Also, the increase in surface energy is another factor that attracts more bacteria.²¹ Thus, the decreased surface roughness and surface energy of the zirconium oxide ALD surfaces of this study resulted in decreased bacterial adhesion.

Surface roughness also has a strong influence on cell attachment. Al-Radha et al reported that after implantation, proteins that mediate cell adhesion, such as fibronectin, are adsorbed onto the implant surface, and these proteins are quickly adsorbed onto rough surfaces, increasing osteoblast adhesion.¹³ Additionally, rougher surfaces influence the cell

anchoring process. Nesbitt et al reported that cells change their morphology and enlarge when settled on rough and hydrophilic surfaces.²² Therefore, as a result of this study, cell proliferation and differentiation were significantly increased due to increased surface roughness after HA deposition. The improved osteoblastic viability in Groups Z and ZH was observed by increased cell attachment, proliferation, and differentiation compared with Group T. It has been shown that zirconium oxide enhances osteoblastic cell adhesion by regulating the gene expression of cells. This regulation could result in a difference in osteoblastic proliferation.²³ This can explain the increased osteoblastic viability of the zirconium oxide deposited groups.

In the contact angle observations, the polar surface energy of Groups TH and ZH was determined to be approximately 5 to 90 times higher than that of Groups T and Z. It has been shown that the polar component of surface energy plays a more important role in cell-titanium interactions.²⁴ Therefore, the higher polar surface energy affected the initial cell attachment and resulted in the increase in cell viability seen in this study.

This study suggests that zirconium oxide and HA deposition on dental implants have the potential to be applied as a surface modification method to inhibit bacterial adhesion and promote osteoblast activity.

However, this study has several limitations in that all experiments were conducted in vitro. The results could differ if it was performed in an oral environment with saliva. Additionally, only a single strain of *S. mutans* was used in this study, but the characteristics of bacteria itself can also affect the results.²⁵ The cell wall composition of Gram-negative bacteria is different from that of *S. mutans*, indicating that bacteria have different surface properties. Therefore, further studies are needed considering these limitations.

Conclusions

In this study, hydroxyapatite and zirconium oxide were deposited on titanium to evaluate the surface properties and resulting biological effects.

The results of this study can be concluded as following:

Zirconium oxide by ALD onto titanium showed decreased adhesion of *S. mutans* and improved osteoblastic viability. HA by RF magnetron sputtering onto titanium showed decreased adhesion of *S. mutans* and increased osteoblastic cell proliferation and cell differentiation. The RF magnetron sputtered HA deposition formed on the zirconium oxide ALD titanium surfaces exhibited the highest antibacterial and osteoblastic properties.

Thus, double-layered hydroxyapatite and zirconium oxide deposited on titanium is proven to have positive influences on the biological properties by the synergistic effect of the two materials.

Acknowledgments

This work was supported by the National Research Foundation of Korea (NRF), grant funded by the Korea government (MSIT) (No. 2022R1A4A1029312), and by the Korean Fund for Regenerative Medicine (KFRM) grant (Ministry of Science and ICT, Ministry of Health & Welfare, 22A0104L1).

Disclosure

The authors report no conflicts of interest in this work.

References

1. Akshaya S, Rowlo PK, Dukle A, et al. Antibacterial coatings for titanium implants: recent trends and future perspectives. *Antibiotics*. 2022;11(12):1719. doi:10.3390/antibiotics11121719
2. Purusothaman M, Sivaprakash V, Bruno AD, et al. Fabrication of TiO₂ nanotubes with effect of water and in-situ condition for biomedical application. *Environ Qual Manage*. 2024;33(4):249–256. doi:10.1002/tqem.22048
3. Xu Y, Meng F. Application of nanomaterials for surface modification of dental implants. *J Mat Process Des*. 2024;8(1):60–68.
4. Schünemann FH, Galárraga-Vinueza ME, Magini R, et al. Zirconia surface modifications for implant dentistry. *Mater Sci Eng*. 2019;98:1294–1305. doi:10.1016/j.msec.2019.01.062
5. Sollazzo V, Pezzetti F, Scarano A, et al. Zirconium oxide coating improves implant osseointegration in vivo. *Dent Mater*. 2008;24(3):357–361. doi:10.1016/j.dental.2007.06.003
6. Johnson RW, Hultqvist A, Bent SF. A brief review of atomic layer deposition: from fundamentals to applications. *Mater Today*. 2014;17(5):236–246. doi:10.1016/j.mattod.2014.04.026

7. Yao L, Wu X, Wu S, et al. Atomic layer deposition of zinc oxide on microrough zirconia to enhance osteogenesis and antibiosis. *Ceram Int*. 2019;45(18):24757–24767. doi:10.1016/j.ceramint.2019.08.216
8. Jo Y, Kim YT, Cho H, Ji M-K, Heo J, Lim H-P. Atomic layer deposition of ZrO₂ on titanium inhibits bacterial adhesion and enhances osteoblast viability. *Int J Nanomed*. 2021;16:1509–1523. doi:10.2147/IJN.S298449
9. Shin JH. *Cellular Effect of Hydroxyapatite Coated Nanotubular Titanium Surface After Heat Treatment*. Department of Dental Science Graduate School, Chonnam National University; 2013.
10. Liao Z, Li J, Su Y, et al. Antibacterial hydroxyapatite coatings on titanium dental implants. *Front Mater Sci*. 2023;17(1):230628. doi:10.1007/s11706-023-0628-x
11. Wang H, Li C, Geng T, et al. Oleic acid-modified layered double hydroxide for Pickering emulsions:(I) Interfacial properties. *Colloids Surf A*. 2024;689:133761. doi:10.1016/j.colsurfa.2024.133761
12. Rožić M, Šegota N, Vukoje M, Kulčar R, Šegota S. Description of thermochromic offset prints morphologies depending on printing substrate. *Appl Sci*. 2020;10(22):8095. doi:10.3390/app10228095
13. Vladescu A, Padmanabhan S, Azem FA, et al. Mechanical properties and biocompatibility of the sputtered Ti doped hydroxyapatite. *J Mech Behav Biomed Mater*. 2016;63:314–325. doi:10.1016/j.jmbbm.2016.06.025
14. Quirynen M, Bollen C. The influence of surface roughness and surface-free energy on supra-and subgingival plaque formation in man: a review of the literature. *J Clin Periodontol*. 1995;22(1):1–14. doi:10.1111/j.1600-051X.1995.tb01765.x
15. Yu P, Wang C, Zhou J, Jiang L, Xue J, Li W. Influence of surface properties on adhesion forces and attachment of streptococcus mutans to zirconia in vitro. *Biomed Res Int*. 2016;2016:1–10. doi:10.1155/2016/8901253
16. Ragab H, Ibrahim F, Abdallah F, et al. Synthesis and in vitro antibacterial properties of hydroxyapatite nanoparticles. *IOSR J Pharm Biol Sci*. 2014;9:77–85.
17. Nesbitt W, Staat R, Rosan B, Taylor K, Doyle R. Association of protein with the cell wall of Streptococcus mutans. *Infect Immun*. 1980;28(1):118–126. doi:10.1128/iai.28.1.118-126.1980
18. Nie Y, Hu C, Kong C. Enhanced fluoride adsorption using Al (III) modified calcium hydroxyapatite. *J Hazard Mater*. 2012;233:194–199. doi:10.1016/j.jhazmat.2012.07.020
19. Murakami A, Arimoto T, Suzuki D, et al. Antimicrobial and osteogenic properties of a hydrophilic-modified nanoscale hydroxyapatite coating on titanium. *Nanomedicine*. 2012;8(3):374–382. doi:10.1016/j.nano.2011.07.001
20. Fujioka-Hirai Y, Akagawa Y, Minagi S, Tsuru H, Miyake Y, Suginaka H. Adherence of Streptococcus mutans to implant materials. *J Biomed Mater Res*. 1987;21(7):913–920. doi:10.1002/jbm.820210707
21. Al-Radha ASD, Dymock D, Younes C, O’Sullivan D. Surface properties of titanium and zirconia dental implant materials and their effect on bacterial adhesion. *J Dent*. 2012;40(2):146–153. doi:10.1016/j.jdent.2011.12.006
22. Zapata KP, Lenis J, Rico P, Ribelles JG, Bolívar F. Determination of synergistic effect between roughness and surface chemistry on cell adhesion of a multilayer Si-Hydroxyapatite coating on Ti6Al4V obtained by magnetron sputtering. *Thin Solid Films*. 2022;760:139489. doi:10.1016/j.tsf.2022.139489
23. Ko H-C, Han J-S, Bächle M, Jang J-H, Shin S-W, Kim D-J. Initial osteoblast-like cell response to pure titanium and zirconia/alumina ceramics. *Dent Mater*. 2007;23(11):1349–1355. doi:10.1016/j.dental.2006.11.023
24. Feng B, Weng J, Yang B, Qu S, Zhang X. Characterization of surface oxide films on titanium and adhesion of osteoblast. *Biomaterials*. 2003;24(25):4663–4670. doi:10.1016/S0142-9612(03)00366-1
25. Murakami A, Arimoto T, Suzuki D, et al. Anti-microbial and osteogenic properties of a hydrophilic-modified nanoscale hydroxyapatite coating on titanium. *Nanomed Nanotechnol Biol Med*. 2012;8(3):374–382.

International Journal of Nanomedicine

Dovepress

Publish your work in this journal

The International Journal of Nanomedicine is an international, peer-reviewed journal focusing on the application of nanotechnology in diagnostics, therapeutics, and drug delivery systems throughout the biomedical field. This journal is indexed on PubMed Central, MedLine, CAS, SciSearch®, Current Contents®/Clinical Medicine, Journal Citation Reports/Science Edition, EMBase, Scopus and the Elsevier Bibliographic databases. The manuscript management system is completely online and includes a very quick and fair peer-review system, which is all easy to use. Visit <http://www.dovepress.com/testimonials.php> to read real quotes from published authors.

Submit your manuscript here: <https://www.dovepress.com/international-journal-of-nanomedicine-journal>